RMetS
Royal Meteorological Society

An analytic model of tropical cyclone wind profiles

Shuai Wang,* Ralf Toumi, Arnaud Czaja and Adrian Van Kan
Department of Physics, Imperial College London, UK

*Correspondence to: S. Wang, Department of Physics, Imperial College London, London, SW7 2AZ, UK.
E-mail: shuai.wang13@imperial.ac.uk

A physically based analytic model (λ model) is presented to describe the wind profile of tropical cyclones in terms of the pressure deficit and a single shape parameter (λ). To test the λ model, an idealized full-physics numerical model is employed to provide wind-profile samples and also to show the influence of environmental temperature and the properties of initial vortices on tropical cyclone size. It is found that the λ model provides an accurate fit of the azimuthal wind profile at the top of the boundary layer. In the simulations, tropical cyclone size is sensitive to sea-surface temperature, upper tropospheric temperature and initial vortex structure. The numerical model confirms the assumed Gaussian distribution with width λ of the moist entropy in the boundary layer. A linear relationship between model cyclone size and $\sqrt{\lambda}$ is found, in agreement with the λ model. The λ model predicts a weak relationship between tropical cyclone size and intensity, as is observed. In addition, the λ model suggests that change in tropical cyclone size should be closely related to angular momentum transport near the boundary layer, as has been found in observations. The good agreement of the λ model with the numerical model shows that the λ model could be a reasonable alternative for characterizing the wind structure of tropical cyclones with only one scaling parameter.

Key Words: tropical cyclone; wind profile; size; moist entropy distribution

Received 9 October 2014; Revised 10 May 2015; Accepted 12 May 2015; Published online in Wiley Online Library

1. Introduction

Tropical cyclone (TC) size is an important feature, setting the extent of coastal flooding, the size of the storm surge and the area threatened by landfall. The importance of TC size is demonstrated by comparing Hurricanes *Sandy* in 2012* and *Bret* in 1999 (Lawrence *et al.*, 2001). As a Saffir–Simpson Hurricane Scale (Simpson and Saffir, 1974) category 3 hurricane, the radius of gale-force wind of Hurricane *Sandy* exceeded 800 km prior to landfall and the storm caused a catastrophic storm surge into the New Jersey and New York coastlines and damage up to an estimated total of 50 billion US dollars. Hurricane *Bret*, on the other hand, was a more intense category 4 hurricane with a radius of gale-force wind of only 140 km. Although the intensity of *Bret* was considerable, damage was reported to be relatively light, totalling an estimated 60 million US dollars. The difference in impacts was caused mainly by the difference in TC size.

There are substantial spatial and temporal variations in TC size. For example, Brand (1972) found geographic and seasonal variations of very large and very small TCs. Merrill (1984) showed that the frequency of large TCs in the North Atlantic reaches a minimum in midsummer and a maximum in October. Furthermore, Western North Pacific TCs are significantly larger than North Atlantic TCs (Liu and Chan, 1999; Chan and Chan, 2012).

Despite the fact that a wide range of observed TC sizes has been recognized, the underlying factors that control both individual storm size and climatological size variation remain mysterious. Changes in TC size are probably induced by environmental factors and the properties of initial vortices. By artificially increasing latent heating in the region of outer rain bands of simulated TCs, Wang (2009) found an outward expansion of winds, which in turn can increase the TC size. Radu *et al.* (2014) suggested that the increase in TC size is proportional to the surface latent heat flux, by altering the air–sea temperature difference. With regards to the properties of initial vortices, Xu and Wang (2010a) suggested that, although the simulated TC intensity at the mature stage may be weakly determined by the initial vortex size, the simulated TC inner-core size is largely dependent on the initial vortex size. Interestingly, this idea is partly confirmed by a statistical study on TC size carried out by Dean *et al.* (2009), who suggested that the size of a given TC may be a function of the geometry of the precursor disturbance that serves to initiate it.

The size of a TC is usually defined using surface pressure and near-surface wind. Merrill (1984) measured size as the average radius of the outer closed isobar. In order to link TC size with potential destructiveness, TC size can also be defined using the near-surface wind speed (Chan and Yip, 2003; Dean *et al.*, 2009; Xu and Wang, 2010a, 2010b; Phibbs and Toumi, 2014; Radu *et al.*, 2014). As a TC is an approximately axisymmetric system, the size can be calculated using the azimuthally averaged wind profile. Based on observational data and gradient wind

*Data available at http://www.nhc.noaa.gov/2012atlan.shtml

equations, Holland (1980) developed one of the most commonly used tangential wind-profile models (hereafter the H model). The H model contains the pressure deficit from the TC centre to the ambient environment (Δp), the Coriolis parameter and two scaling parameters, A and B. B is a measure describing the shape of wind profiles. An increase in B indicates that the wind profile becomes more 'flat' than the original. The H model has been successfully implemented in TC forecasting and risk models. By fitting the wind data to the H model, one can easily calculate the TC size. However, the H model is partly based on a statistical fit to observational data and it is difficult to get an analytical solution to TC size by giving a threshold wind speed. A new theoretical wind-profile model is presented here, which overcomes these limitations.

The main goal of this article is to derive a new TC model for the wind profile based on the Emanuel (1986, hereafter E86) air–sea interaction theory. The new model should be able to provide an analytical solution for TC size, which could be beneficial to further TC size studies. To test the new theoretical model, four sets of sensitivity experiments on TC size are conducted using a full-physics idealized numerical model. The sensitivity experiments can also show the influence of environmental temperature and the properties of initial vortices on TC size, which is the other goal of this study.

The following section introduces the idealized model set-up, sensitivity experiment design and the derivation of the new theoretical model. Section 3 presents the simulated TC intensity and size and the relationship between the size changes caused by different factors and the moist entropy distribution at the top of the boundary layer (TBL). Physical insights from this study are discussed in section 4. Section 5 summarizes the overall findings.

2. Method

2.1. Model set-up and experiment design

In order to reduce the case-specific impacts, we utilized a full-physics Advanced Research Weather Research and Forecasting (WRF) model to simulate ideal TCs. The model was configured with two domains: a coarse mesh of 15 km horizontal grid spacing and a two-way and vortex-following nested domain of 3 km grid spacing. The domains were square and were of side 4500 km (300 $\times$ 300 grid points) and 1503 km (501 $\times$ 501 points). There were 31 σ-levels in the vertical with a higher resolution located in the boundary layer and a model top of 50 hPa. All the experiments lasted for 8 days.

All experiments were initialized with an axisymmetric vortex. The initially horizontal wind field $V_0(r)$ of the vortex was specified with an idealized vortex wind model following Chan and Williams (1987):

$$V_0(r) = V_{\mathrm{m}} \left(\frac{r}{R_{\mathrm{m}}}\right) \exp \frac{1}{b}\left[1 - \left(\frac{r}{R_{\mathrm{m}}}\right)^b\right], \qquad (1)$$

where r is the radius from the vortex centre, V_{m} the initial maximum wind, R_{m} the radial position of V_{m} and b a factor that can determine the shape of the wind profile. In all of the experiments, b was set as 0.33 (Hill and Lackmann, 2009). Vertical structure was introduced to the horizontal wind field by decaying it linearly with height (Rotunno and Emanuel, 1987):

$$V(r,z) = V_0(r)\frac{(z^* - z)}{z^*}. \qquad (2)$$

In (2), $v = 0$ at $z = z^*$ and we let $v = 0$ for $z > z^*$ and set z^* as 20 km.

The environmental sounding profile was specified as the mean tropical sounding in 'hurricane season' (July–October) of Jordan (1958) and the background flow was set as 0 m s^{-1}. After an initial vortex was added into the environment, the temperature field was computed from thermal wind balance, geopotential heights were set in terms of gradient wind balance and the pressure perturbations were calculated by the hydrostatic equation (Kwok and Chan, 2005). Note that these adjustments may change the initial central pressure if the initial wind field is changed. At any given σ level, the relative humidity was set as a constant value with Jordan's sounding, so the temperature and pressure perturbation induced a specific humidity adjustment.

The idealized experiments were conducted over an ocean-only domain. Model experiments were performed on an f-plane and the Coriolis parameter f was set constant at 20°N ($f \approx 5 \times 10^{-5}$ s^{-1}). All experiments used the following set-up: Tiedtke cumulus parametrization scheme (Tiedtke, 1989; Zhang *et al.*, 2011) on the 15 km grids only, WSM six-class graupel scheme (Hong and Lim, 2006) of microphysical processes, the Rapid Radiative Transfer Model scheme (Mlawer *et al.*, 1997) to estimate the effects of long-wave radiation and the Dudhia (1989) implementation for short-wave radiation. The surface layer used a similarity scheme based on Monin–Obukhov with a Carslon–Boland viscous sub-layer and standard similarity functions, along with the Yonsei University scheme (Hong and Lim, 2006) for parametrization of processes in the planetary boundary layer. The lateral boundary condition for the outermost domain was specified by Jordan's sounding.

In the control experiment (CTRL), the sea-surface temperature (SST) was fixed at 28°C and the initial vortex maximum wind speed was 20 m s^{-1} at a radius of 75 km from the vortex centre. Four sets of sensitivity experiments were designed to investigate the sensitivity of TC size to environmental temperature and initial vortex parameters (Table 1). Emanuel *et al.* (2013) showed that, according to the reanalysis data and weather station records, in the past 30 years there has been a 2 K decrease in tropical tropopause temperature and this cooling has influenced Atlantic hurricane activity. On the other hand, Hill and Lackmann (2011) found that projected upper tropospheric warming in the next 100 years might change the TC intensity. However, how the TC size responds to the upper-tropospheric temperature has not been studied specifically. The near-surface heat exchange is important to TC change and we consider the importance of SST to quantify its impact on TC size. The size of a mature TC may also be determined by the initial size of the TC (Rotunno and Emanuel, 1987; Cocks and Gray, 2002; Xu and Wang, 2010a; Chan and Chan, 2015). In each experiment, only one of SST, upper tropospheric (150–300 hPa) temperature (T_{UT}), V_{m} and R_{m} in the initial wind field was changed (Figure 1).

Even though we fixed the b parameter in (1), changes in V_{m} or R_{m} can still result in a shape change in the wind profile. The H model is employed here to describe these initial shape changes. With the three fitting parameters, the H model gives excellent approximations (Pearson correlation coefficient, $R^2 > 0.99$) to the numerical model profiles. The B values and the profiles in Figure 1(b) show that the whole wind profile is changed when altering V_{m} and R_{m} in (1). More discussion about their influence on TC size is provided in section 4.

To verify that the simulated cyclones are fully developed, we compared the simulated intensity with the TC maximum

Table 1. List of simulation names for sensitivity experiments. The increments are compared with CTRL.

Simulation name	ΔSST (°C)	ΔT_{UT} (°C)	ΔV_{m} (m s^{-1})	ΔR_{m} (km)
SST(+1)	+1	0	0	0
SST(−1)	−1	0	0	0
T_{UT}(+2)	0	+2	0	0
T_{UT}(−2)	0	−2	0	0
V_{m}(+5)	0	0	+5	0
V_{m}(−5)	0	0	−5	0
R_{m}(+25)	0	0	0	+25
R_{m}(−25)	0	0	0	−25

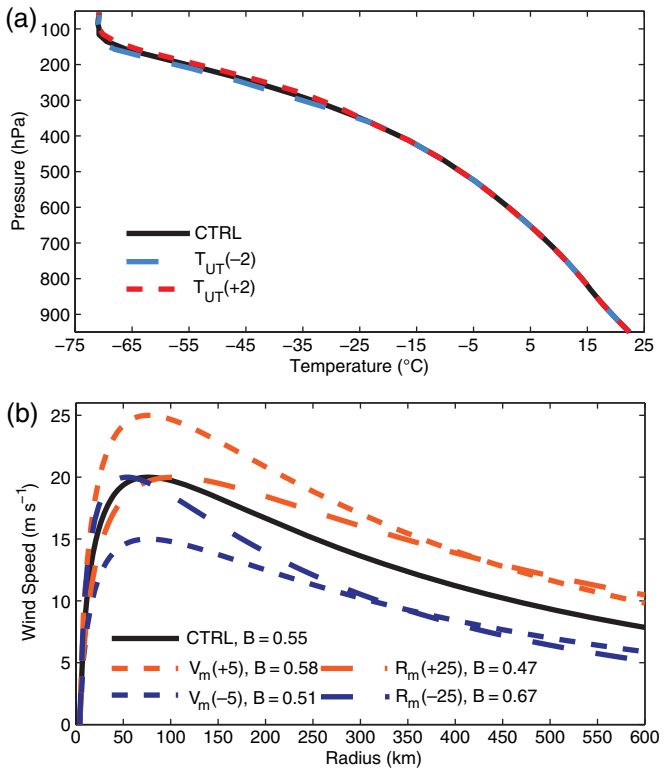

Figure 1. Initial set-up of (a) air temperature soundings and (b) the speed and radial position of maximum wind in CTRL, $V_m(\pm 5)$ and $R_m(\pm 25)$ experiments.

potential intensity (MPI) of Emanuel (1995):

$$V_{\mathrm{mpi}} = (1-\gamma)\sqrt{C_{\mathrm{p}}\left(T_{\mathrm{s}} - T_{\mathrm{out}}\right)\frac{C_K}{C_{\mathrm{D}}}\left(\ln\theta_{\mathrm{e}}^{*} - \ln\theta_{\mathrm{e}}\right)}, \tag{3}$$

where V_{mpi} is the potential maximum near-surface wind speed and also the approximate MPI if defining TC intensity with near-surface winds, γ the coefficient reflecting the typical relationship between gradient winds and actual near-surface winds ($\gamma = 0.2$), C_{p} the heat capacity at constant pressure, T_{s} the ocean surface temperature, T_{out} the mean outflow temperature, C_K the exchange coefficient for enthalpy, C_{D} the drag coefficient, θ_{e}^{*} the saturation equivalent potential temperature evaluated under the eyewall of a developed TC at sea level and θ_{e} the boundary-layer equivalent potential temperature. Note that the coefficient γ was not considered by Emanuel (1995). Theoretically, if a cyclone becomes fully developed, its intensity should be close to the MPI but not exceed it.

2.2. *The λ model for wind-speed distribution*

E86 set up an air–sea interaction theory for a steady-state TC. Based on this theory, we have obtained analytical solutions for wind-speed distribution and hence TC size, which we describe briefly below.

For a steady-state axisymmetric TC over an ocean with constant temperature, we shall assume that above the boundary layer and except in the outflow at large radii, the moist entropy (s_{m}) and angular momentum per unit mass (M) are conserved. They are defined as

$$\begin{aligned} s_{\mathrm{m}} = &\left\{\left(1-q_t\right)C_{\mathrm{pd}} + q_t C_l\right\}\ln\left(\frac{T}{T_{\mathrm{o}}}\right) \\ &- \left(1-q_t\right)R_{\mathrm{d}}\ln\left(\frac{p_{\mathrm{d}}}{p_{\mathrm{o}}}\right) + q_{\mathrm{v}}\frac{L_{\mathrm{v}}}{T} - q_{\mathrm{v}}R_{\mathrm{v}}\ln RH, \end{aligned} \tag{4}$$

$$M = rV + \frac{1}{2}fr^2, \tag{5}$$

where V is the tangential velocity, f the Coriolis parameter, C_l the heat capacity of liquid water, C_{pd} the heat capacity of dry air, T the air temperature, p_{d} the partial pressure of dry air, RH the relative humidity, R_{d} the gas constant of dry air, R_{v} the gas constant of water vapour, L_{v} the latent heat of vaporization, q_{v} the specific humidity of water vapour, $q_t = q_{\mathrm{v}} + q_l$ with q_l the specific humidity of condensate water, T_{o} the arbitrary reference temperature (set as 273.15 K) and p_{o} the arbitrary reference partial pressure of dry air (set as 1000 hPa). The reader is referred to Pauluis *et al.* (2010) for a derivation of (4).

Hydrostatic balance and gradient wind balance are assumed in the free atmosphere as well and may be written as

$$\alpha\frac{\partial p}{\partial z} = -g, \tag{6}$$

$$\alpha\frac{\partial p}{\partial r} = \frac{V^2}{r} + fV, \tag{7}$$

where g is the acceleration of gravity, p the pressure and α the specific volume.

The cornerstone of E86 theory, which shows that knowledge of s_{m} as a function of r allows one to determine M as a function of r at the TBL, may be written as

$$-r^2\frac{\partial s_{\mathrm{m}}}{\partial r}\Delta T = \frac{1}{2}\frac{\partial M^2}{\partial r}, \tag{8}$$

where $\Delta T = T_{\mathrm{tbl}} - T_{\mathrm{out}}$, T_{tbl} is the temperature at the TBL and T_{out} is the temperature in the outflow region.

A key step in our work is that we propose a solution to s_{m} in (8):

$$s_{\mathrm{m}}(r) = \Delta s_{\mathrm{m}} \mathrm{e}^{-r^2/(2\lambda^2)} + s_{\mathrm{env}}, \tag{9}$$

where Δs_{m} is the moist entropy increment from the ambient environment to the TC centre and s_{env} the moist entropy in the ambient environment. Equation (9) is a Gaussian distribution and the physical meaning of λ here is the horizontal width of moist entropy at the TBL. This choice is motivated by the excellent Gaussian fit (more details in section 3.2).

Assuming that the azimuthal velocity at the centre of a TC is zero and assuming further that ΔT is a constant, by virtue of (9) one can integrate (8) to obtain

$$M(r) = \mu\sqrt{2\lambda^2(1-\epsilon) - r^2\epsilon}, \tag{10}$$

in which $\mu = \sqrt{2\Delta T \Delta s_{\mathrm{m}}}$ and $\mathrm{e}^{-r^2/(2\lambda^2)}$ is replaced with ϵ for simplicity.

Using (5) in (7) and eliminating M by virtue of (10), (7) may be written as

$$\alpha\frac{\partial p}{\partial r} = \frac{M^2}{r^3} - \frac{f^2}{4}r = \mu^2\left[\frac{2\lambda^2}{r^3}(1-\epsilon) - \frac{1}{r}\epsilon\right] - \frac{f^2}{4}r. \tag{11}$$

Neglecting horizontal variations in α, this equation can be integrated with respect to radius to obtain

$$p(r) = \frac{\mu^2}{2\alpha}\frac{1-\epsilon}{\ln\epsilon} - \frac{f^2r^2}{8\alpha} + C, \tag{12}$$

in which C is a constant of integration. Equation (12) shows that the presence of TC introduces a pressure perturbation $p'(r)$:

$$p'(r) = \frac{\mu^2}{2\alpha}\frac{1-\epsilon}{\ln\epsilon}, \tag{13}$$

which, at the centre of the TC, is simply $p'(0) = \Delta p$, where

$$\Delta p = \frac{\mu^2}{2\alpha}. \tag{14}$$

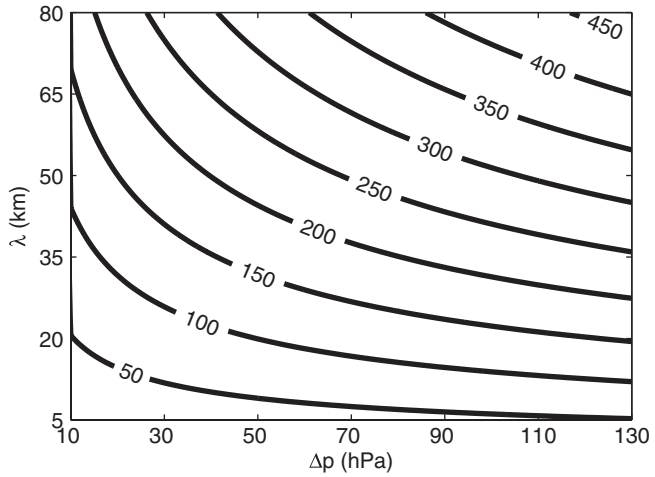

Figure 2. Radius of damaging-force wind (km) as a function of horizontal width (λ, km) of moist entropy at the TBL and pressure deficit (Δp, hPa) computed from (17) for $V_{\rm th} = 26\,{\rm m\,s^{-1}}$, $f = 5 \times 10^{-5}\,{\rm s^{-1}}$ and $\alpha = 0.91\,{\rm m^3 kg^{-1}}$.

Note that this equation can be interpreted physically by rewriting it as $\alpha \Delta p = \Delta T \Delta s_{\rm m}$, equating the work of expansion ($\alpha \Delta p$) with the heat added by air–sea fluxes at the sea surface times an efficiency ($T_{\rm s} \Delta s_{\rm m} \times \Delta T / T_{\rm s}$).

Using (10) and (14) in (5), one may obtain an analytical solution for tangential velocity at the TBL:

$$V = \sqrt{2\alpha \Delta p} \sqrt{\frac{2\lambda^2}{r^2}(1-\epsilon) - \epsilon} - \frac{1}{2} fr. \tag{15}$$

Substituting an arbitrary threshold wind velocity $V_{\rm th}$ in this equation and neglecting terms involving ϵ at a radius much larger than λ, (15) can be simplified as

$$\frac{f}{2} {r_{\rm th}}^2 + V_{\rm th} r_{\rm th} - 2\lambda \sqrt{\alpha \Delta p} = 0, \tag{16}$$

where $r_{\rm th}$ is the radius defined with $V_{\rm th}$ at the TBL. The value of this radius is then given by solving (16) analytically:

$$r_{\rm th} = \frac{\sqrt{{V_{\rm th}}^2 + 4f\lambda\sqrt{\alpha \Delta p}} - V_{\rm th}}{f}. \tag{17}$$

Equation (17) shows how the size of the TC depends on its pressure deficit (Δp) and the width of the entropy distribution in the boundary layer (λ), for a given wind threshold. The only scaling parameter is λ, whereas the widely used H model has two scaling parameters. This model for the radial wind profile is referred to in the following as the λ model. Its prediction of TC size is illustrated in Figure 2. At fixed Δp, the size defined by any wind threshold increases with λ. Conversely, at fixed λ, a greater pressure deficit results in a larger TC. The λ model makes an important prediction: for a fully developed tropical cyclone, its size largely depends on λ and varies weakly with Δp. We test this prediction with a full-physics numerical model in the next section.

3. Results

3.1. Intensity and MPI comparisons

Figure 3 shows the time series of the minimum surface pressure ($p_{\rm min}$). In CTRL, the initial central pressure is about 965 hPa. $p_{\rm min}$ decreases by almost 80 hPa in the first three simulation days and reaches a minimum value on the fourth simulation day. In the next four days, $p_{\rm min}$ reaches a relatively steady state. The pressure changes in $T_{\rm UT}(\pm 2)$ (Figure 3(a)) are similar to CTRL. However, the pressure differences in SST(± 1) are significant (Figure 3(b)). The small shifts at the beginning in $V_{\rm m}(\pm 5)$ (Figure 3(c)) and $R_{\rm m}(\pm 25)$ (Figure 3(d)) are caused by the adjustment processes. The pressure in $V_{\rm m}(-5)$ attains its maximum value about 24 h later than in CTRL and $V_{\rm m}(+5)$. The pressure difference between CTRL and $R_{\rm m}(\pm 25)$ is not noticeable. Figure 4 shows the time series of maximum wind at a height of 10 m ($V_{\rm 10max}$). $V_{\rm 10max}$ in CTRL increases by more than 40 m s^{-1} in the first three simulation days and attains its maximum value on the fourth simulation day. $V_{\rm 10max}$ tendencies in other sensitivity experiments are similar to CTRL. According to the changes in $p_{\rm min}$ and $V_{\rm 10max}$, we defined the developing stage as running from simulation hours 0–72 and the mature stage from simulation hours 73–192.

The simulated intensity $V_{\rm 10max}$ is compared with the MPI in Table 2. According to the MPI calculation (3), $V_{\rm mpi}$ for the environment specified with Jordan's sounding is 67 m s^{-1}. In $V_{\rm m}(\pm 5)$ and $R_{\rm m}(\pm 25)$, $V_{\rm mpi}$ is the same because the environment is unchanged. The difference between $V_{\rm mpi}$ and $V_{\rm 10max}$ in CTRL, $V_{\rm m}(\pm 5)$ and $R_{\rm m}(\pm 25)$ is smaller than 3 m s^{-1}. $V_{\rm mpi}$ increases in SST($+1$) and $T_{\rm UT}(-2)$. However, the response in those experiments compared with CTRL is less in the model than predicted by the upper limit of MPI. $V_{\rm mpi}$ in experiments SST(-1) and $T_{\rm UT}(+2)$ decreases and there is a corresponding drop in $V_{\rm 10max}$. The response in those experiments compared with CTRL is again much less than predicted by MPI. One consequence of this is that for the SST(-1) experiment $V_{\rm mpi}$ is surprisingly less than $V_{\rm 10max}$.

3.2. λ model and the simulations

The relevance of (9) to the numerical model entropy in CTRL at simulation hour 150 is assessed in Figure 5. The λ model assumed a well-mixed boundary layer, so the vertically averaged entropy (over the lowest six levels, approximately 600 m) is calculated using (4). There is an excellent fit of the Gaussian function to the entropy distribution in the later stage of the cyclone in the control simulation (Figure 5(a)). As the Gaussian distribution of moist entropy is the foundation of the λ model, we take a further step to verify the validity of this assumption. For comparison purposes, one of the other possible solutions to $s_{\rm m}$ in (8) is given as an example:

$$s_{\rm m}(r) = \Delta s_{\rm m} {\rm e}^{-r/\lambda} + s_{\rm env}. \tag{18}$$

Equation (18) is in an exponential form. By taking the natural logarithm of the percentage change of $s_{\rm m}(r)$, (9) and (18) can be transformed to parabolic and linear forms, respectively. Figure 5(b) shows that a parabolic fit gives a much better result, which further supports the choice (9).

Figure 6 shows the time series of R^2 from the Gaussian fit in all experiments. The adjustment from an initially assumed exponential distribution to a Gaussian occurs within 24 h. The R^2 at the simulation hour 24 is close to 0.96; it increases slightly in the next 48 h. There is also an excellent fit for all experiments (mean $R^2 = 0.99$) from hour 48 onwards, even before the cyclone is fully developed. The noise becomes stronger in the last 24 h, but R^2 is still greater than 0.96.

Having shown that (9) can describe the simulated moist entropy distribution, we can apply this assumption to predict the speed distribution as a function of Δp and λ using (15). Deriving the central pressure at the TBL and using an ambient pressure of 916 hPa, Figure 7 shows a good fit ($R^2 = 0.94$) of the λ model at simulation hour 150 in CTRL. All essential features of the wind distribution are captured: the radial position and value of maximum wind, the dramatic increase in velocity from the centre to the eyewall and the gradual decrease outside the eyewall. There is a small shift outwards near the maximum and underestimation at larger radii. With Δp and *RMW* from simulations, the H model gives a good approximation ($R^2 = 0.91$) to the wind profile as well. However, the H model overestimates the wind speed outside the eyewall at this time. For the λ

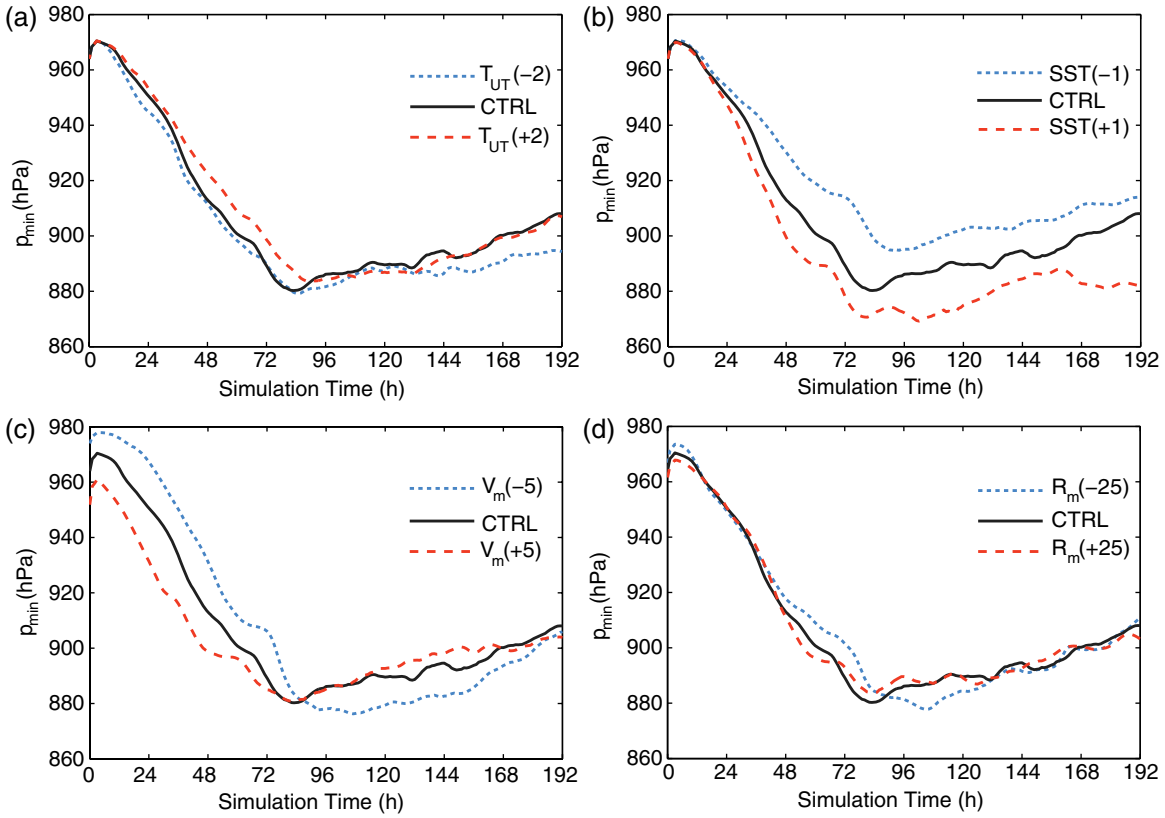

Figure 3. Time series of minimum surface pressure for (a) $T_{UT}(\pm 2)$, (b) SST(± 1), (c) $V_m(\pm 5)$ and (d) $R_m(\pm 25)$ experiments, with application of a moving average smoother. The span for the moving average is 5.

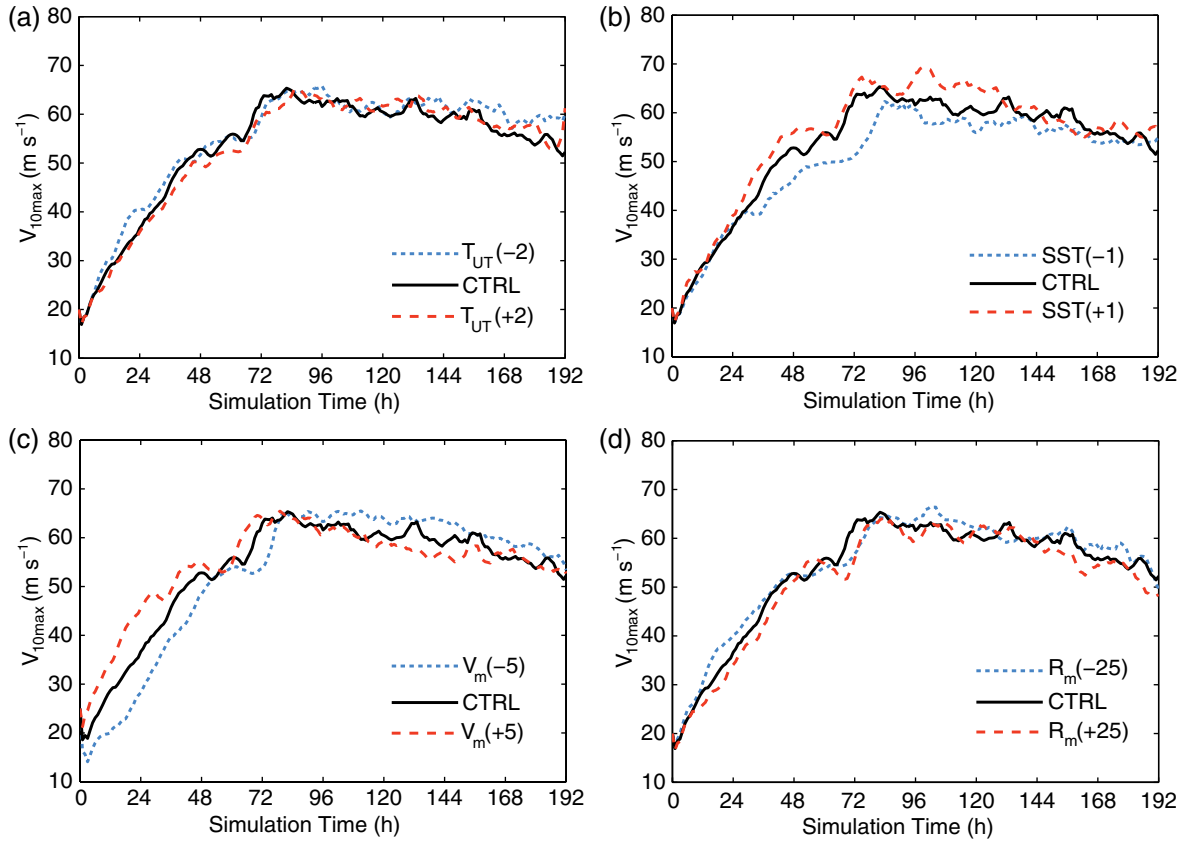

Figure 4. As in Figure 3, but for maximum wind speed.

model, Figure 8 shows that there is also a good fit for all experiments (mean $R^2 = 0.89$) from hour 72 onwards when the cyclone is fully developed. The comparison between λ and H models in Figure 8 shows that the λ model seems as good as the extensively used H model (mean $R^2 = 0.89$), but uses one parameter fewer.

3.3. *Size and λ*

We measure TC size as the radius of hurricane-force wind (≈ 33 m s^{-1}; *R*33), radius of damaging-force wind (≈26 m s^{-1}; *R*26), radius of gale-force wind (≈17 m s^{-1}; *R*17) and *RMW*. All the size measurements are based on the azimuthally averaged tangential

Table 2. Comparison of maximum wind speed (units m s^{-1}) between MPI theory (V_{mpi}) and simulation results (V_{10max}).

Simulation name	V_{mpi}	V_{10max}	$V_{mpi} - V_{10max}$
CTRL	67	65	+2
$V_m(+5)$	67	65	+2
$V_m(-5)$	67	65	+2
$R_m(+25)$	67	64	+3
$R_m(-25)$	67	66	+1
SST(+1)	76	69	+7
SST(−1)	57	62	−5
$T_{UT}(+2)$	66	65	+1
$T_{UT}(-2)$	68	66	+2

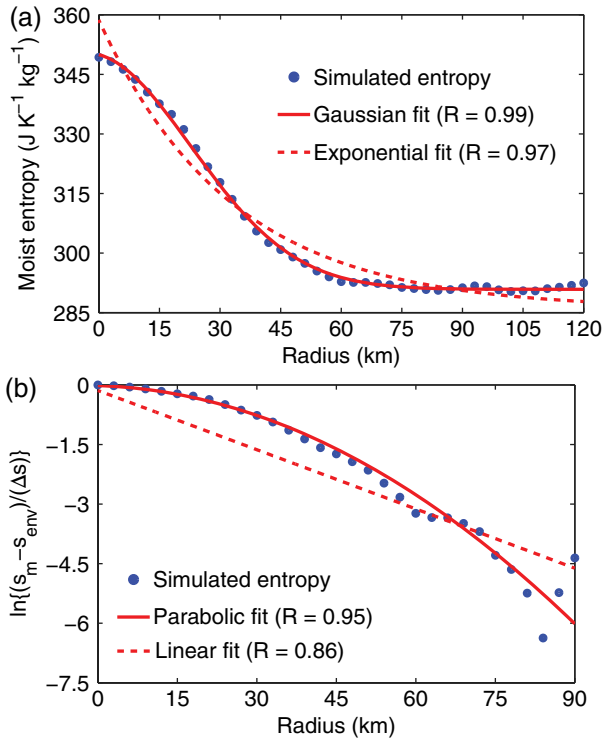

Figure 5. (a) Gaussian and exponential fits of moist entropy and (b) parabolic and linear fits of the natural logarithm of the percentage change xof moist entropy in CTRL at simulation hour 150. In the Gaussian fit, $\Delta s_m = 59.6\,\mathrm{J\,K^{-1}\,kg^{-1}}$, $\lambda = 25.8$ km and $s_{env} = 290.7\,\mathrm{J\,K^{-1}\,kg^{-1}}$. In the exponential fit, $\Delta s_m = 80.0\,\mathrm{J\,K^{-1}\,kg^{-1}}$, $\lambda = 32.8$ km and $s_{env} = 286.1\,\mathrm{J\,K^{-1}\,kg^{-1}}$. In the parabolic and linear fits, $\lambda = 26.8$ and 20.1 km, respectively, and $\ln\{(s_m - s_{env})/\Delta s\}$ is calculated from simulation results.

wind (Chan and Yip, 2003; Dean *et al.*, 2009; Xu and Wang, 2010a, 2010b). The size variations of *R*33 and *R*17 are similar to those of *R*26, so only the results of *R*26 and *RMW* are shown.

Figure 9 shows that, at the mature stage (simulation hour 150), clear changes in the distance of damaging-force wind occur in all sets of experiments. In addition, they are essentially axisymmetric, which allows us to use the *R*26 value. Figure 9 shows that TC size is sensitive to upper tropospheric temperature, SST and initial vortex structure. Figure 10 depicts the time evolution of *R*26 in all experiments. *R*26 in CTRL increases significantly in the developing stage and its size becomes relatively steady after exceeding about 100 km. Figure 10(a) shows that *R*26 in $T_{UT}(-2)$ starts to increase earlier and is always greater than in CTRL and $T_{UT}(+2)$. *R*26 in SST(±1) (Figure 10(b)) increases at almost the same time, but the rise of SST(+1) is much larger and *R*26 at hour 192 is about 170 km, which is the largest size in all the experiments. Figure 10(c) shows that *R*26 of $V_m(+5)$ begins to rise about 20 h earlier than that in $V_m(-5)$ and, the earlier the increase happens, the larger the final size. However, *R*26 begins to increase earlier in $R_m(-25)$ than $R_m(+25)$ but there is a larger cyclone in $R_m(+25)$ at the mature stage. These time series show the same variations in TC size at the mature stage as Figure 9,

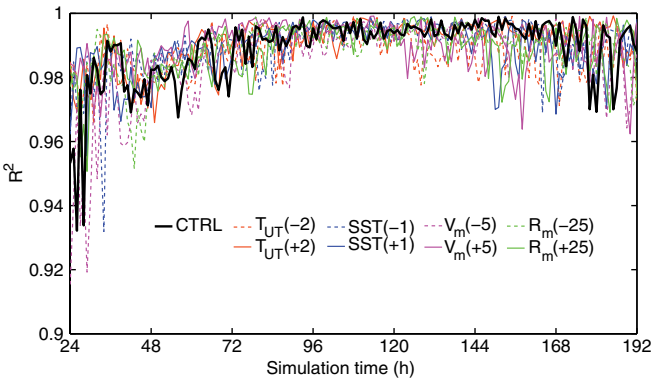

Figure 6. R^2 from entropy fitting from simulation hours 24–192.

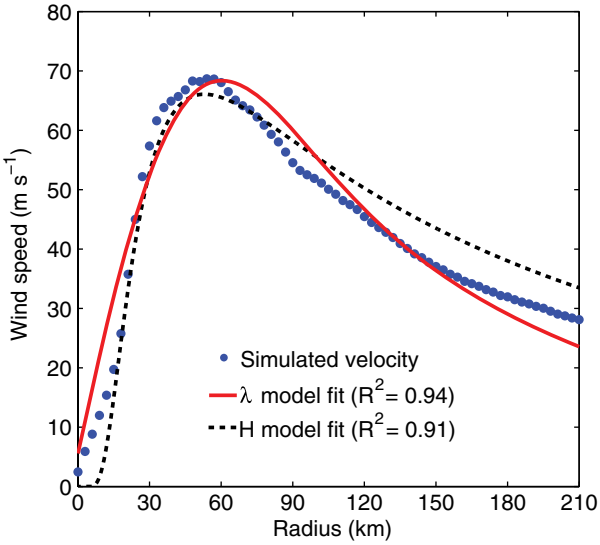

Figure 7. Fit of tangential velocity at the TBL in CTRL at simulation hour 150. In the λ model, $\lambda = 34.0$ km and in the H model, $B = 1.5$. The air density is fixed at 1.1 kg m^{-3} and ambient pressure at the TBL is 916 hPa.

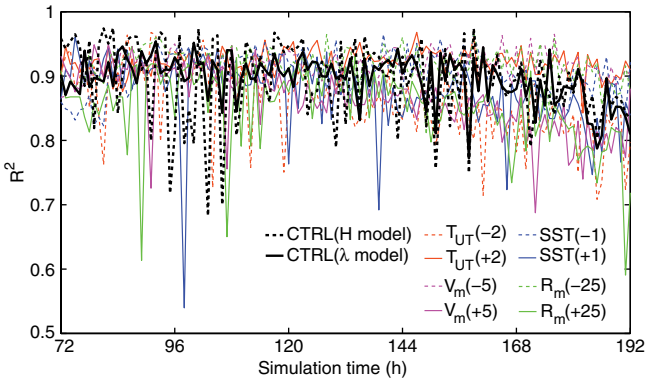

Figure 8. R^2 from the tangential velocity fit at the TBL from simulation hours 72–192. The black dashed line represents R^2 by using the H model as a fitting function. All other lines show R^2 with (17) in the λ model as a fitting function. The central pressure and radius of maximum wind are calculated at each time step.

which suggests that the changes in size shown in Figure 9 are persistent.

As for *RMW* (Figure 11), the changes are noiser than the variations in *R*26. In the first simulation day, *RMW* drops significantly to about 30 km and then increases gradually to around 60 km. The size evolution and response to environmental conditions are similar to *R*26 at the later stage of development.

Figure 12 shows the time series of λ obtained from fitting the Gaussian distribution to the simulated moist entropy. In $T_{UT}(\pm2)$ and SST(±1), the initial λ is the same, whereas small shifts (about

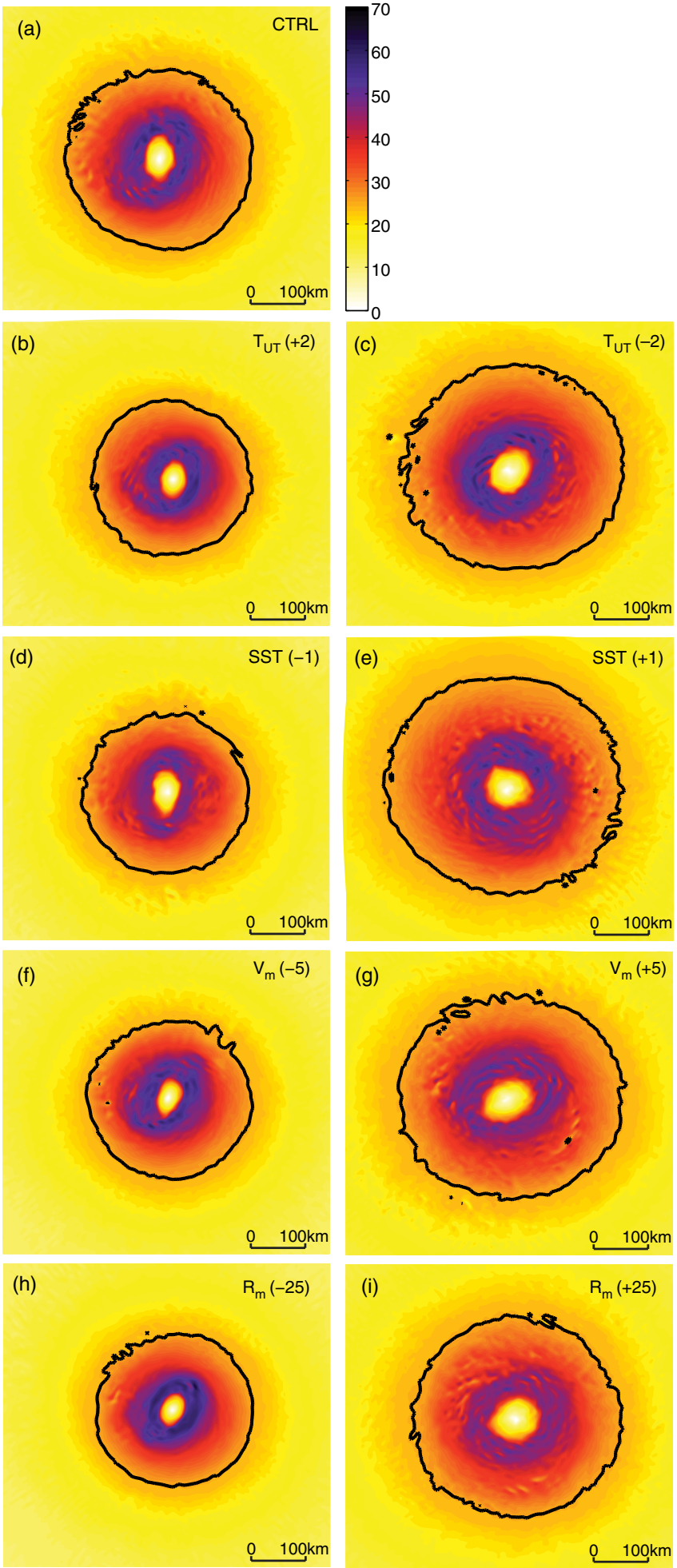

Figure 9. Model-simulated wind speed ($m\,s^{-1}$) at a height of 10 m at hour 144 for (a) CTRL, (b) $T_{UT}(+2)$, (c) $T_{UT}(-2)$, (d) SST(−1), (e) SST(+1), (f) $V_m(-5)$, (g) $V_m(+5)$, (h) $R_m(-25)$ and (i) $R_m(+25)$. The black contours show the TC size defined with $R26$. All panels have the same horizontal scale.

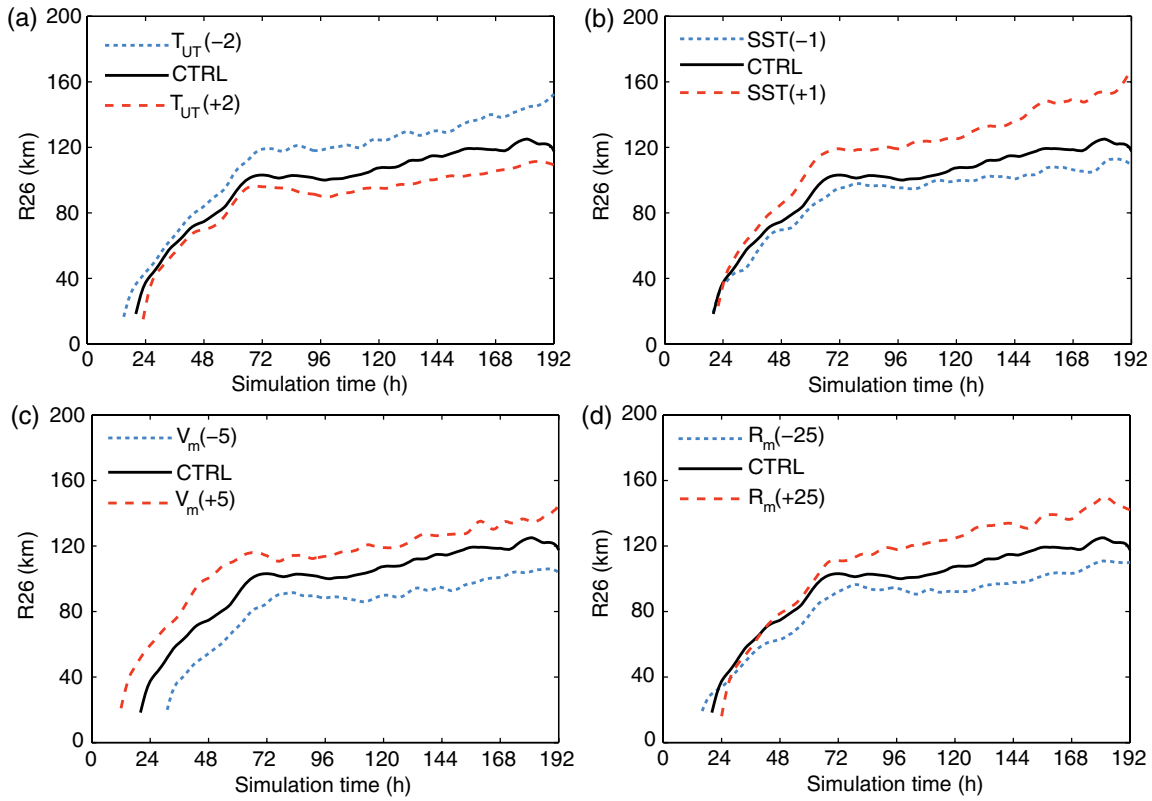

Figure 10. As in Figure 3, but for the radius of damaging-force wind.

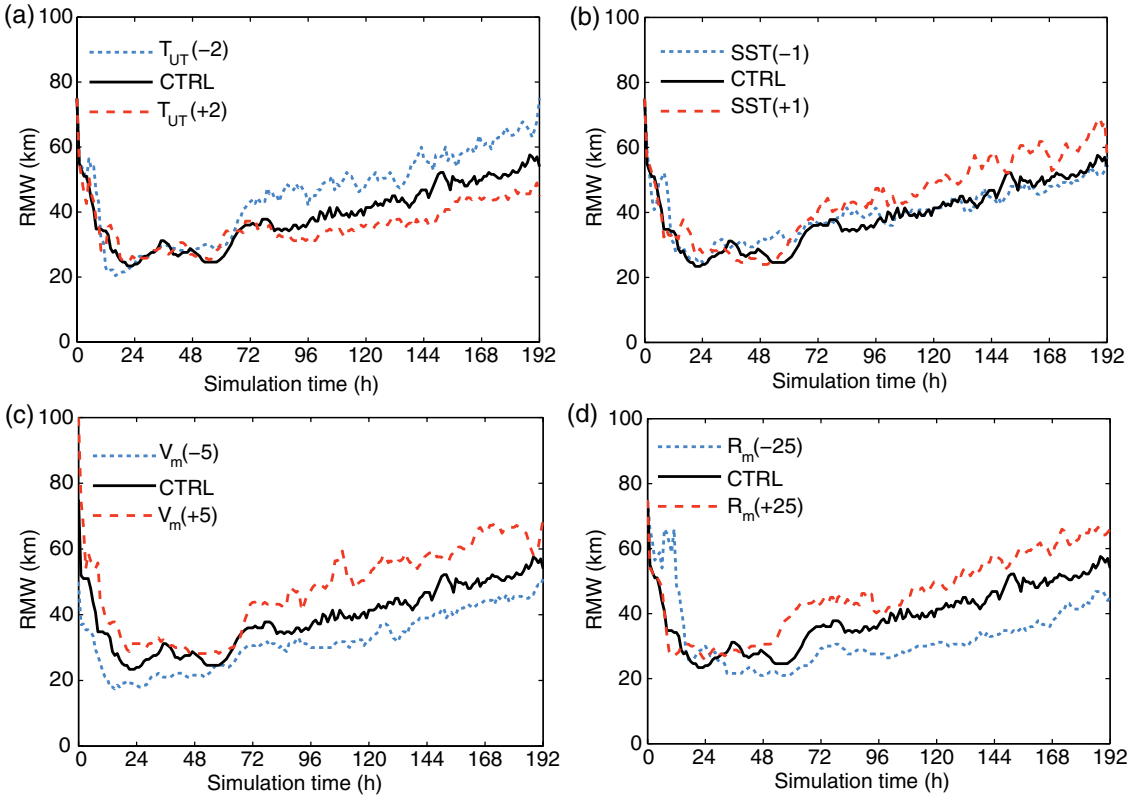

Figure 11. As in Figure 3, but for the radius of maximum wind.

±4 km) in $R_m(\pm 25)$ and $V_m(\pm 5)$ are generated due to changes in initial wind profiles. At the developing stage, the changes in λ are noisy but the amplitude of the noise decreases with time. In the mature stage, every set of experiments shows clear differences in λ and λ increases gradually at this stage, just like the size. Comparing Figure 12 with Figures 10 and 11, one can see that the changes in λ are more similar to the variations in *RMW* and at the mature stage there should be a positive correlation between TC size and λ.

3.4. *Linear relationship between size and* $\sqrt{\lambda}$

Based on (17), there is a predicted simple relationship for the radii and λ in the special case $V_{th} = 0$:

$$r_{th} \propto \sqrt{\lambda}. \tag{19}$$

We test (19) by comparing $\sqrt{\lambda}$ from entropy fitting at the mature stage in all experiments with *R*26, a more common TC

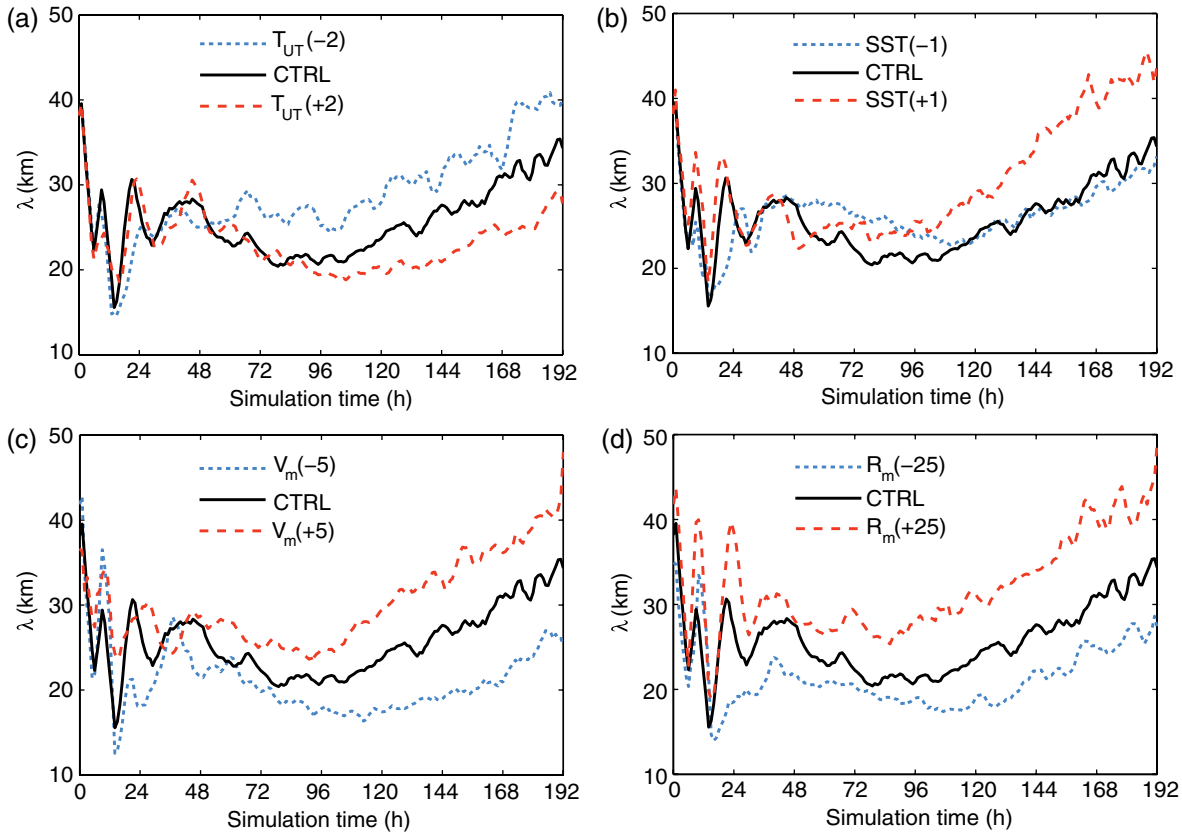

Figure 12. As in Figure 3, but for λ from the moist entropy fitting with (9).

size definition, instead of the radius of vanishing wind, which is difficult to find in the simulations due to noise. Figure 13(a) shows that larger cyclones correspond to larger $\sqrt{\lambda}$ ($R^2 = 0.84$). The R^2 of $R17$ and $R33$ with $\sqrt{\lambda}$ are 0.80 and 0.74, respectively. Figure 13(b) and (c) compares λ with the other two fitting coefficients (Δs_m and s_{env}) in (9). There is no good relationship between size and the entropy increment from the ambient environment to the TC centre or the environmental entropy. Furthermore, although we did not solve for *RMW* analytically, the empirical linear relationship ($R^2 = 0.90$) is even better than that between $R26$ and $\sqrt{\lambda}$ (Figure 14).

3.5. $\sqrt{\lambda}$ and angular momentum

To understand further the physical process related to the change in size, the relationship between $\sqrt{\lambda}$ and the symmetric radial angular momentum flux (SAMF) is shown in Figure 15. SAMF is defined as the sum of the symmetric relative angular momentum flux and the symmetric Coriolis torque. The reader is referred to Chan and Chan (2013) for a detailed derivation of SAMF. The SAMF here is the hourly mean flux within the boundary layer and within $R17$, which is the most outwards size considered in this article. A negative value means that angular momentum is imported towards the centre. Figure 15 shows a good linear relationship ($R^2 = 0.74$) between SAMF and $\sqrt{\lambda}$ and suggests that angular momentum transport in the boundary layer is related to change in TC size.

4. Discussion

We find that intensity changes are only small for our range of experiments. SST does cause certain variations in intensity after the second simulation day, but the V_{10max} difference gradually reduces with time at the mature stage (Figure 4(b)). Figure 4(c) shows that a cyclone starting with a weak vortex results in a slightly more intense cyclone at the mature stage. However, Rotunno and Emanuel (1987) found that an initially weak vortex leads to a weaker cyclone, which is contrary to our finding. We note that the initial maximum wind speed of the weak vortex in this study is 15 m s^{-1}, whereas the initial maximum wind speed in their work was only 2 m s^{-1}, which may be too weak for a vortex to become fully developed.

In general, the variations in simulated intensity are consistent with the theoretical MPI results. However, compared with CTRL, the response in SST($\pm$1) and $T_{UT}(\pm2)$ is smaller than MPI predicts and this is expected, as the MPI is intended as a plausible upper limit, whereas the full model includes atmospheric negative feedbacks such as enhanced radiation and frictional loss. SST($-$1) produces winds 5 m s^{-1} stronger than the potential maximum wind speed. The cause for this is not clear; however, we note that the fluctuation of the maximum wind speed is about $\pm$ 5 m s^{-1} in the mature state and this 'superintensity' is also found by others (e.g. Persing and Montgomery, 2003).

The λ model, according to the fitting results (Figures 5–8), is a promising solution to describing the tangential velocity distribution. The single-parameter λ model seems as good as the H model with two scaling parameters. It is also pleasing to note that there is a physical basis (the thermal wind balance (8)) in the λ model. We have developed the model further to explore TC size. One can identify three different factors in TC size from (17): firstly the pressure drop from the ambient environment to the eye, secondly the Coriolis parameter and thirdly the distribution of moist entropy at the TBL given by λ. According to (17), the cyclone should shrink with increasing latitude. To support this argument, an additional set of simulations was performed. We ran the CTRL experiment on the f-plane at 20°N, 30°N and 40°N and the results show that the average $R26$ within the mature stage is 109, 98 and 94 km, respectively. This result shows qualitative agreement with (17). However, we note that the change in $R26$ caused by varying f is only half or less than half the value (17) suggests for the radius of vanishing wind. The changes in $R17$ and $R33$ with latitude are similar to those of $R26$. In a model study, Chavas and Emanuel (2014) also found that the radius of vanishing wind increases nearly linearly with $1/f$. Dean *et al.* (2009) shows that, according to E86 theory, the upper limitation

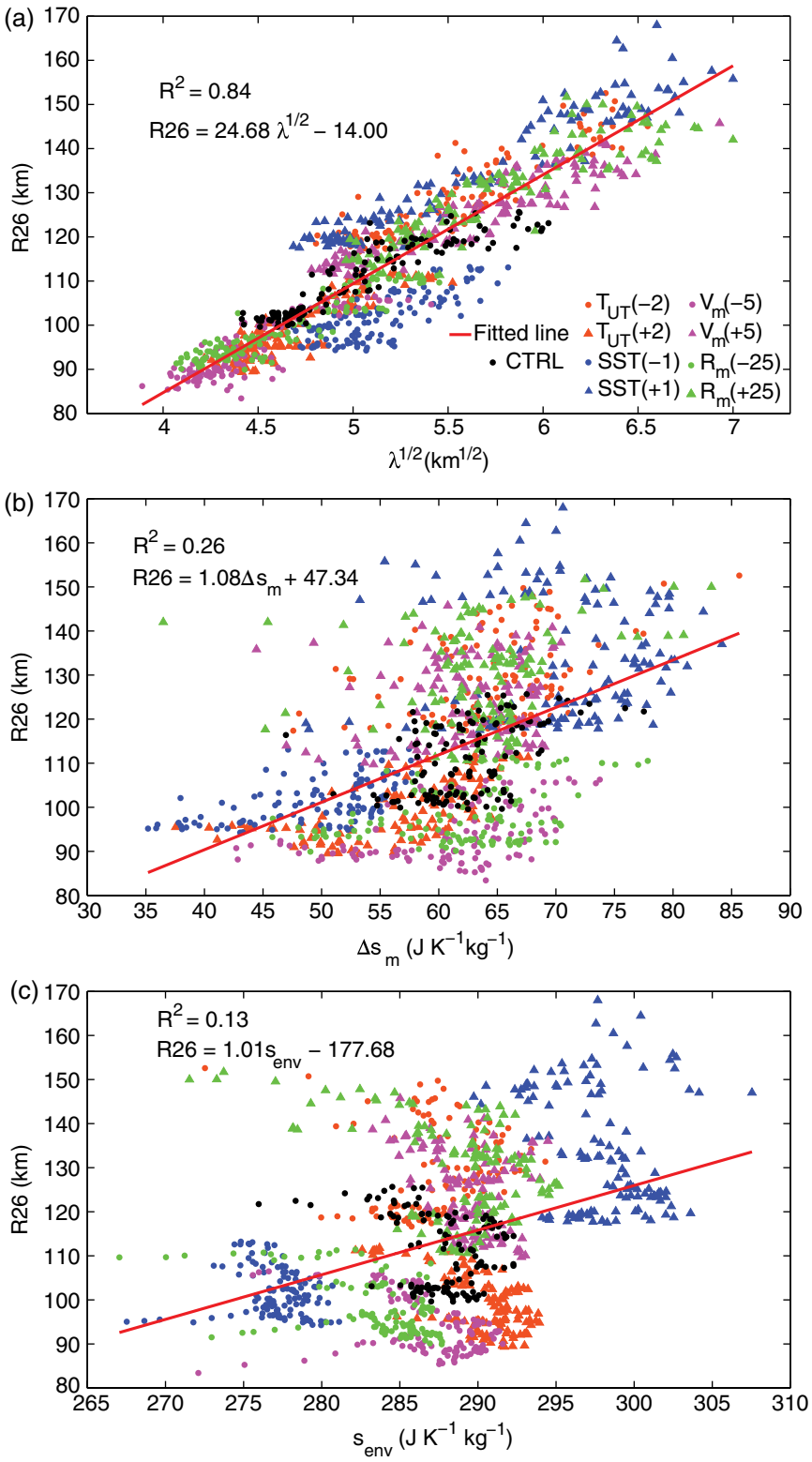

Figure 13. Linear regression between $R26$ and (a) $\sqrt{\lambda}$, (b) Δs_m and (c) s_{env}. All the markers are hourly outputs from simulation hours 72–192 of all nine experiments.

on overall storm size is proportional to $1/f$. However, these studies are not consistent with other observational studies (Weatherford and Gray, 1988; Kimball and Mulekar, 2004), which suggests that TCs at higher latitude have greater size. Interestingly, Smith *et al.* (2011) and Chan and Chan (2014) show that an optimum region may exist for a TC to attain a maximum size. To investigate the reason for those disagreements, more simulation experiments need to be performed.

One should be aware that the starting assumption of this model is a solution to the moist entropy distribution at the TBL. The assumed initial moist entropy is in an exponential distribution and, in the developing stage, the entropy distribution turns into a Gaussian form in less than 24 h. Since this Gaussian solution to the moist entropy is similar to the solution to the one-dimensional diffusion equation, we speculate that the process in which the distribution of moist entropy turns from an exponential to a Gaussian form is dominated by horizontally turbulent diffusion in the boundary layer, down the gradient of high to low entropy. This might be represented by a diffusivity coefficient through a flux gradient relationship. However, we found that the hourly eddy radial entropy flux has no relationship with λ, so this explanation of the Gaussian shape appears unlikely.

We have identified that TC size is sensitive to environmental temperature and initial vortex structure (Figures 9–11). A cold upper troposphere, warm SST and a large and intense initial vortex are all favourable to TC size growth. By altering

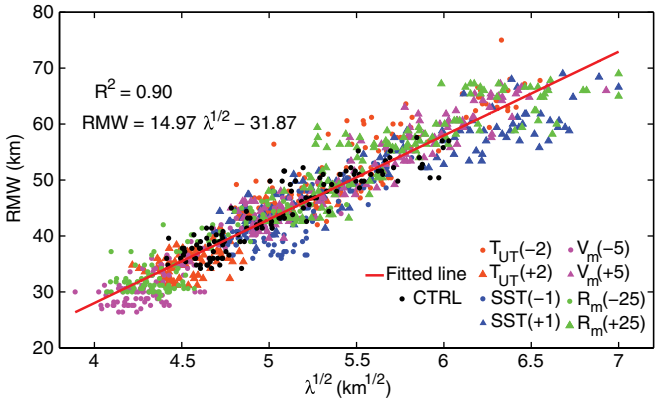

Figure 14. As in Figure 13, but for the radius of maximum wind.

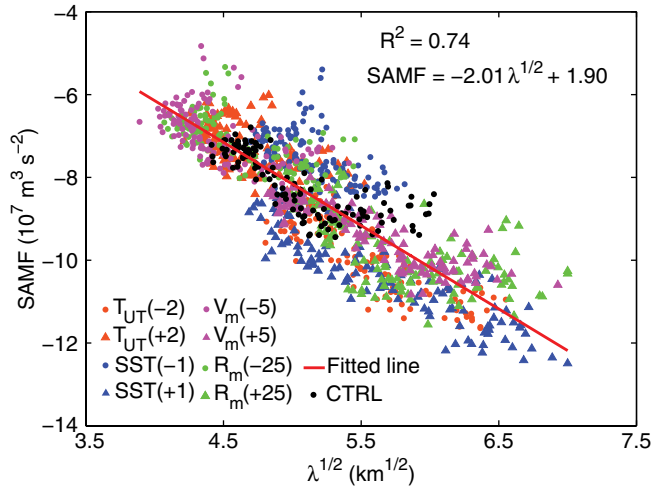

Figure 15. As in Figure 13, but for the symmetric radial angular momentum flux in the boundary layer.

upper tropospheric (150–300 hPa) temperature, the outflow temperature is changed. E86 indicates briefly that outflow temperature may be negatively related to the radius of the outermost closed isobar. Although we use a different size definition, the results agree. This relationship between size and upper tropospheric temperature suggests that there could be trends in the size of TCs, not just the intensity (Emanuel *et al.*, 2013). Increased SST creates more significant air–sea temperature contrast and results in stronger latent energy transfer from the ocean to the air, as found by Radu *et al.* (2014). The cyclone size is sensitive to the initial vortex structure. This finding is in agreement with the model simulations by Xu and Wang (2010a) and Chan and Chan (2014, 2015). However, it should be noted that, by changing the initial *RMW* or V_m, the *B* value also changes in the H model (Figure 1(b)), which means that the whole wind profile changes. That causes a compounded effect of inner- and outer-core winds on TC size, namely one cannot conclude that the inner-core wind structure is more important to size than the outer one based on just these experiments ($R_m(\pm 25)$ and $V_m(\pm 5)$). Nevertheless, the λ model is a good description of the mature stages in all these experiments, which is the main finding of our work.

Although the SST is held constant throughout the simulation so that the TC has a constant energy reservoir, the intensity (V_{10max}) does decrease slightly (Figure 4). In contrast to this, the cyclone size continues to increase in all experiments (Figures 10 and 11). A possible explanation is that the increase in TC size results in a reduction in intensity through angular momentum conservation. According to MPI theory, there is an upper limit on TC intensity for this environment. However, it seems plausible that such a limit does not exist for TC size as long as a stable energy supply exists.

For all experiments, the changes in intensity are small and sometimes hardly noticeable. However the changes in TC size are much larger and clearer. This suggests only a weak relationship between intensity and size. The λ model provides a potential theoretical explanation for this from (17) when $V_{th} = 0$:

$$r_{th} \propto \sqrt[4]{\Delta p}. \tag{20}$$

One can see that the radius of vanishing wind is only proportional to the fourth root of the pressure deficit, whereas the dependence on the width of the entropy distribution is proportional to $\sqrt{\lambda}$. A similar prediction of *R26* is shown in Figure 2 and also supported by previous climatological studies showing that size is only weakly correlated with intensity (Frank and Gray, 1980; Merrill, 1984; Weatherford and Gray, 1988; Chan and Chan, 2012).

The assumed entropy depends on three variables in (9): the environmental entropy, the difference in entropy between the environment and the core and the width of the entropy distribution, λ. However, only λ shows a clear impact on the size, not the entropy in the ambient environment or the contrast between the environment and the central areas (Figure 13). The entropy distribution for the different experiments changes mainly in the central area, with a radius of less than 100 km (Figure 5). This may be the reason that λ has a closer relationship to *RMW* than *R26*.

Another explanation of the good relationship between λ and *RMW* can be explored by expanding the theoretical analysis. Taking the derivative of tangential wind in (15) with respect to *r* and making it equal to zero, one obtains

$$\left[\epsilon_m\left(\frac{RMW}{\lambda^2}+\frac{2}{r}+4\frac{\lambda^2}{RMW^3}\right)-4\frac{\lambda^2}{RMW^3}\right]^2 = \frac{f^2}{\mu^2}\left[\frac{2\lambda^2}{RMW^2}-\left(\frac{2\lambda^2}{RMW^2}+1\right)\epsilon_m\right], \tag{21}$$

where $\epsilon_m = e^{-RMW^2/(2\lambda^2)}$.

According to a scale analysis with the typical values of *RMW* ($\sim 10^4$ m), *f* ($\sim 10^{-4}$ s^{-1}), μ ($\sim 10^2$ J$^{1/2}$ kg$^{-1/2}$) and λ ($\sim 10^4$ m), the right-hand part of the above equation can be neglected and (21) can be written as

$$\epsilon_m\left(\frac{RMW}{\lambda^2}+\frac{2}{RMW}+4\frac{\lambda^2}{RMW^3}\right)-4\frac{\lambda^2}{RMW^3}=0. \tag{22}$$

Equation (22) has no analytic solution. However, it does indicate that *RMW* is a function of λ alone. In contrast, *R26* depends on λ and, albeit weakly, on Δ*p*. This may further explain the better relationship between λ and *RMW* than for *R26*.

Figures 13(a) and 14 show that TC size is well correlated with $\sqrt{\lambda}$, which suggests that we can understand size in terms of $\sqrt{\lambda}$. $\sqrt{\lambda}$ is a property of the moist entropy distribution at TBL, and according to our derivation starting from E86, the moist entropy is a function of angular momentum per unit mass. This means that TC size should be related to the radial angular momentum distribution and transport near the boundary layer. This argument agrees with Chan and Chan (2013), who showed that, based on observations and re-analysis data, the SAMF in the lower troposphere is important with regard to the change in TC size. As for our simulations, the good correlation between $\sqrt{\lambda}$ and SAMF in the boundary layer shown in Figure 15 further supports the connection between change in TC size and angular momentum transport in the boundary layer.

5. Conclusions

A new analytic tropical cyclone model, the λ model, has been derived. The λ model correctly depicts the tangential velocity profile at the TBL. Based on the λ model, the TC size is

a function of the distribution of moist entropy at the TBL given by λ, the pressure drop from the ambient environment to the eye, and the Coriolis parameter. In simulations, we found that SST, upper troposphere temperature and initial vortex structure can all affect the subsequent TC size. These size changes caused by different factors all have good relationships with the width of the Gaussian moist entropy distribution as shown by the λ model.

With regards to TC size and intensity, we find that, unlike the intensity prediction based on MPI theory, it seems that there is no upper limit for TC size provided there is sufficient energy support from the ocean. The increase in TC size at the mature stage also causes a slight drop in intensity. In addition, a weak relationship between TC size and intensity is confirmed in the simulations and this relationship can be understood with the λ model.

One may be able to predict TC size by understanding what sets the width λ. As E86 shows that the moist entropy is a function of the angular momentum per unit mass, we show that size may be highly related to angular momentum import within the boundary layer, which is consistent with the observations reported by Chan and Chan (2013). On an f-plane, angular momentum flux is controlled by the local angular momentum and radial wind and the latter may be the key factor in TC size change. The relatively simple single-scaling-parameter λ model presented appears to capture these essential features in a physical manner.

Acknowledgement

We thank the CSC Imperial Scholarship Programme and BP Environmental Technology Programme for their support, as well as the referees for their helpful comments.

References

Brand S. 1972. Very large and very small typhoons of the western North Pacific Ocean. *J. Meteorol. Soc. Jpn.* **50**: 332–341.

Chan KTF, Chan JCL. 2012. Size and strength of tropical cyclones as inferred from QuikSCAT data. *Mon. Weather Rev.* **140**: 811–824.

Chan KTF, Chan JCL. 2013. Angular momentum transports and synoptic flow patterns associated with tropical cyclone size change. *Mon. Weather Rev.* **141**: 3985–4007.

Chan KTF, Chan JCL. 2014. Impacts of initial vortex size and planetary vorticity on tropical cyclone size. *Q. J. R. Meteorol. Soc.* **140**: 2235–2248.

Chan KTF, Chan JCL. 2015. Impacts of vortex intensity and outer winds on tropical cyclone size[J]. *Q. J. R. Meteorol. Soc.* **141**: 525–537.

Chan JCL, Williams RT. 1987. Analytical and numerical studies of the beta-effect in tropical cyclone motion. Part 1: Zero mean flow. *J. Atmos. Sci.* **44**: 1257–1265.

Chan JCL, Yip CKM. 2003. Interannual variations of tropical cyclone size over the western North Pacific. *Geophys. Res. Lett.* **30**: 2267, doi:10.1029/2003GL018522.

Chavas DR, Emanuel K. 2014. Equilibrium tropical cyclone size in an idealized state of axisymmetric radiative convective equilibrium. *J. Atmos. Sci.* **71**: 1663–1680.

Cocks SB, Gray WM. 2002. Variability of the outer wind profiles of western North Pacific typhoons: Classifications and techniques for analysis and forecasting. *Mon. Weather Rev.* **130**: 1989–2005.

Dean L, Emanuel KA, Chavas DR. 2009. On the size distribution of Atlantic tropical cyclones, *Geophys. Res. Lett.* **36**: L14803, doi:10.1029/2009GL039051.

Dudhia J. 1989. Numerical study of convection observed during the Winter Monsoon Experiment using a mesoscale two-dimensional model. *J. Atmos. Sci.* **46**: 3077–3107.

Emanuel KA. 1995. Sensitivity of tropical cyclones to surface exchange coefficients and a revised steady-state model incorporating eye dynamics. *J. Atmos. Sci.* **52**: 3969–3976.

Emanuel K, Solomon S, Folini D, Davis S, Cagnazzo C. 2013. Influence of tropical tropopause layer cooling on Atlantic hurricane activity. *J. Clim.* **26**: 2288–2301.

Frank WM, Gray WM. 1980. Radius and frequency of 30 kt winds around tropical cyclones. *J. Appl. Meteorol.* **19**: 219–223.

Hill KA, Lackmann GM. 2009. Influence of environmental humidity on tropical cyclone size. *Mon. Weather Rev.* **137**: 3294–3315.

Hill KA, Lackmann GM. 2011. The impact of future climate change on TC intensity and structure: A downscaling approach. *J. Clim.* **24**: 4644–4661.

Holland G. 1980. An analytic model of the wind and pressure profiles in hurricanes. *Mon. Weather Rev.* **108**: 1212–1218.

Hong SY, Lim JOJ. 2006. The WRF Single-Moment 6-Class Microphysics Scheme (WSM6). *J. Korean Meteorol. Soc.* **42**: 129–151.

Jordan C. 1958. Mean soundings for the West Indies area. *J. Meteorol.* **15**: 91–97.

Kimball SK, Mulekar MS. 2004. A 15-year climatology of North Atlantic tropical cyclones. Part I: Size parameters. *J. Clim.* **17**: 3555–3575.

Kwok JHY, Chan JCL. 2005. The influence of uniform flow on tropical cyclone intensity change. *J. Atmos. Sci.* **62**: 3193–3212.

Lawrence MB, Avila LA, Beven JL, Franklin JL, Guiney JL, Pasch RJ. 2001. Atlantic hurricane season of 1999. *Mon. Weather Rev.* **129**: 3057–3084.

Liu KS, Chan JCL. 1999. Size of tropical cyclones as inferred from ERS-1 and ERS-2 data. *Mon. Weather Rev.* **127**: 2992–3001.

Merrill RT. 1984. A comparison of large and small tropical cyclones. *Mon. Weather Rev.* **112**: 1408–1418.

Mlawer EJ, Taubman SJ, Brown PD, Iacono MJ, Clough SA. 1997. Radiative transfer for inhomogeneous atmospheres: RRTM, a validated correlated-k model for the longwave. *J. Geophys. Res.* **102**: 16663–16682, doi:10.1029/97JD00237.

Pauluis O, Czaja A, Korty R. 2010. The global atmospheric circulation in moist isentropic coordinates. *J. Clim.* **23**: 3077–3093.

Persing J, Montgomery MT. 2003. Hurricane superintensity. *J. Atmos. Sci.* **60**: 2349–2371.

Phibbs S, Toumi R. 2014. Modeled dependence of wind and waves on ocean temperature in tropical cyclones. *Geophys. Res. Lett.* **41**: 7383–7390, doi: 10.1002/2014GL061721.

Radu R, Toumi R, Phau J. 2014. Influence of atmospheric and sea-surface temperature on the size of hurricane Catarina. *Q. J. R. Meteorol. Soc.* **140**: 1778–1784.

Rotunno R, Emanuel K. 1987. An air–sea interaction theory for tropical cyclones. Part 2: Evolutionary study using a nonhydrostatic axisymmetric numerical model. *J. Atmos. Sci.* **44**: 542–561.

Simpson RH, Saffir H. 1974. The hurricane disaster potential scale. *Weatherwise* **27**: 169.

Smith RK, Schmidt CW, Montgomery MT. 2011. An investigation of rotational influences on tropical-cyclone size and intensity. *Q. J. R. Meteorol. Soc.* **137**: 1841–1855.

Tiedtke M. 1989. A comprehensive mass flux scheme for cumulus parameterization in large-scale models. *Mon. Weather Rev.* **117**: 1779–1800.

Wang Y. 2009. How do outer spiral rain bands affect tropical cyclone structure and intensity? *J. Atmos. Sci.* **66**: 1250–1273.

Weatherford CL, Gray WM. 1988. Typhoon structure as revealed by aircraft reconnaissance. Part II. Structural variability. *Mon. Weather Rev.* **116**: 1044–1056.

Xu J, Wang Y. 2010a. Sensitivity of the simulated tropical cyclone inner-core size to the initial vortex size. *Mon. Weather Rev.* **138**: 4135–4157.

Xu J, Wang Y. 2010b. Sensitivity of tropical cyclone inner-core size and intensity to the radial distribution of surface entropy flux. *J. Atmos. Sci.* **67**: 1831–1852.

Zhang C, Wang Y, Hamilton K. 2011. Improved representation of boundary layer clouds over the Southeast Pacific in ARW-WRF using a modified Tiedtke cumulus parameterization scheme. *Mon. Weather Rev.* **139**: 3489–3513.

